

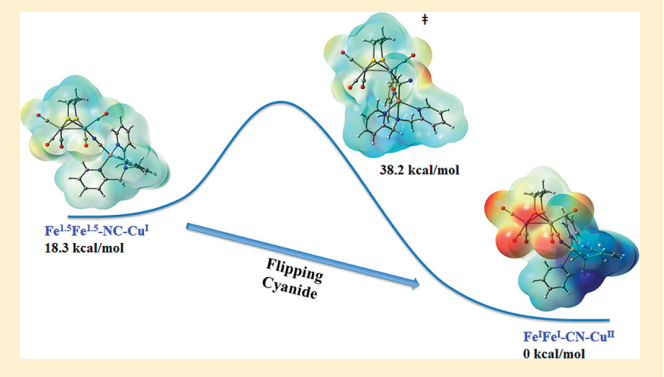
# Cyanide Docking and Linkage Isomerism in Models for the Artificial [FeFe]-Hydrogenase Maturation Process

Debangsu Sil, Zachary Martinez, Shengda Ding, Nattamai Bhuvanesh, Donald J. Darensbourg, <sup>10</sup> Michael B. Hall,\* and Marcetta Y. Darensbourg\*

Department of Chemistry, Texas A & M University, College Station, Texas 77843, United States

Supporting Information

ABSTRACT: Linkage isomerization of the cyanide on the [2Fe] subsite of the [FeFe]-H<sub>2</sub>ase active site was reported to occur during the docking of various synthetic diiron complexes onto a carrier protein, apo-HydF, as the initial step for the artificial maturation of the [FeFe]-H2ase enzyme (Berggren et al., Nature, 2013, 499, 66-70). An investigation of our triiron organometallic models (FeFe-CN/NC-Fe') revealed that, once a Fe-CN-Fe connection is formed, high barriers prevent such cyanide linkage isomerization (Chem. Sci., 2016, 7, 3710-3719). To explore effects of variable oxidation states of the receiver unit, we introduce copper(I/ II) fragments, precedented in Holm's models of cytochrome c oxidase to induce cyanide isomerization (Cu-CN/NC-Fe), to



the diiron synthetic analogues of [FeFe]-H<sub>2</sub>ase. For comparison, a zinc variant of the cytochrome c oxidase model is also examined. According to the oxidation state of copper, a cyanide flip was induced during the formation of both Zn-NC-Cu and FeFe-CN-Cu complexes. Density functional theory calculations are used to predict the mechanisms for such linkage isomerization and account for optimal conditions including oxidation states of metals, spin states, and solvation. These results on synthetic paradigms imply a role for oxidation state control of cyanide isomerization during hydrogenase active site assembly.

### INTRODUCTION

As well as in their attempts to model the active site structures and catalytic ability of the [NiFe]- and [FeFe]-hydrogenases, synthetic organometallic chemists have found challenges in the production of hybrid enzymes, first reported for the [FeFe]-H<sub>2</sub>ase in 2013. 1-10 Berggren et al. observed that synthetic [2Fe] subunits of the form  $(\mu\text{-SCH}_2\text{XCH}_2\text{S})[\text{Fe}(\text{CO})_2\text{CN}]_2^{2-}$ could be loaded onto bacterial Thermotoga maritima HydF devoid of the natural apparatus for making the cyano-ironcarbonyl units.<sup>5</sup> A subsequent transfer of the synthetic diiron complex to apo-HydA1 from Chlamydomonas reinhardtii algae resulted in loss of a CO group and two isomerizations, as noted in the cartoon representation of Figure 1; these are (1) a linkage isomerization of the cyanide that bridges the [4Fe4S] cluster to the 2Fe subsite and (2) a rearrangement of the diiron unit into the form that creates an open site on the distal iron replete with pendant N base within the dithiolate that connects the two irons. The X in the SCH<sub>2</sub>XCH<sub>2</sub>S linker on hybrid enzymes was varied as X = NH, CH<sub>2</sub>, O, and S; wild-type enzyme activity was observed only for the amine. Such studies provided unequivocal evidence of the pendant base effect in directing protons to the distal iron, a feature already accepted as key to the mechanism of proton reduction in [FeFe]-H<sub>2</sub>ase. A recent report on the X-ray structure of HydF from the thermophilic bacterium Thermosipho melanesiensis revealed that its [4Fe4S] cluster is coordinated by three cysteines and a

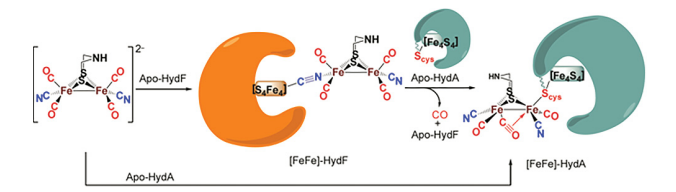


Figure 1. Representation of the loading of an Fe<sup>I</sup>Fe<sup>I</sup> model of the diiron subsite of [FeFe]-H2ase onto the apo-HydF maturation protein.5 Its subsequent transfer to apo-HydA results in the characteristic [FeFe]-hydrogenase enzyme. The orange and blue shapes are used as cartoons for the protein chain in HydF and HydA, respectively.

glutamate residue. It was observed that the glutamate was replaced by substrates (the synthetic [2Fe] subunits) during the maturation process.<sup>7</sup> The study also proposed ( $\mu$ adt)[Fe(CO)<sub>2</sub>CN]<sub>2</sub><sup>2-</sup> (adt = azapropanedithiolate) to be the native [2Fe] unit based on the ability of  $(\mu$ -adt)[Fe- $(CO)_2CN]_2^{2-}$ -bound HydF to mature to HydA and similarities in its FTIR spectra to those of the native HydF active intermediate.

Received: April 26, 2018 Published: July 12, 2018

While the cyanide diatomic ligand is used in classic studies of enzyme inhibition and metal-binding sites, its use as a unit to dock the synthetic [FeFe] subunit to the [4Fe4S] cluster of the protein chain during maturation was unexpected. The linkage isomerism, deduced from detailed spectroscopic characterization of the [FeFe]-HydF complex, is important as the possibility of cyanide as a mooring agent broadens its currently presumed function as a facilitator for Fe $^{\rm I}/{\rm Fe}^{\rm II}$  redox changes. In addition, favorable H-bonding interactions stabilize the [FeFe]- and [NiFe]-H2ases active sites within their protein superstructures.

A recent study also showed that modification of the amino acid residues in the secondary sphere, near the cyanide ligand and close to the [4Fe4S] unit, influences the catalytic bias toward either  $H_2$  production or  $H_2$  oxidation, depending on the pH.

Preliminary studies of a set of cyanide-bridged [FeFe]-CN-Fe complexes as models of the [FeFe]-NC-[4Fe4S] arrangement in the [FeFe]-HydF found no cyanide flips occurring on mixing of precursors. Consistent with an earlier report of a large group of cyanide-bridged organometallic complexes by Vahrenkamp et al., including sets of linkage isomers derived from different synthetic routes, the direction of the CN link was completely determined by the precursors. Calculations using DFT found a high kinetic barrier for CN isomerization in [FeFe]-CN-Fe  $\rightleftharpoons$  [FeFe]-NC-Fe units, rather than thermodynamics, accounting for the stability of the onceformed cyanide bridge. This indicates that the flipping of the CN- ligand is likely induced by the receiver end, i.e., an iron of the [4Fe4S] unit in the case of [FeFe]-HydF.

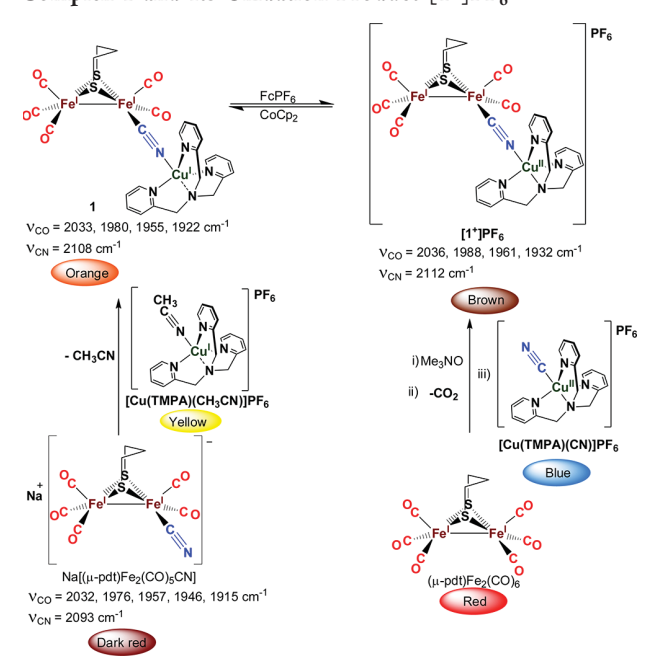
Among reports of CN<sup>-</sup> linkage isomerism occurring during the course of adduct formation are those of particular relevance to bioinorganic chemistry. Holm<sup>16–20</sup> and Karlin<sup>21</sup> explored cyanide-bridged copper-iron complexes as biomimetics of the cyanide-inhibited cytochrome c oxidase, whose ultimate copper-cyanide-iron arrangement was rationalized by the rule of hard/soft interactions, rather than the starting orientation of the cyanide donor. Herein, we describe cyanide-bridged complexes of the diiron using copper, in its two oxidation states, as a surrogate for the iron-sulfur cluster of HydF. At the Fe<sup>I</sup>Fe<sup>I</sup> redox level of the diiron cyano unit the FeFe-CN-Cu<sup>II</sup> arrangement was obtained via two chemical routes, one of which contains a cyanide flip as the bridge is formed. In an extension of the Holm study and for verification of our computational protocol, we also explored the Zn-NC-Cu adducts that exhibit flips of the cyanide ligand from its orientation in precursor donors. Density functional theory (DFT) calculations have examined the possible mechanism of such cyanide flips along with other geometric changes.

### ■ RESULTS AND DISCUSSION

**Synthesis and Characterization.** The synthetic routes to the target complexes of this study are shown in Schemes 1 and 2. Treatment of a dark red CH<sub>3</sub>CN solution of Na[( $\mu$ -pdt)Fe<sub>2</sub>(CO)<sub>5</sub>CN]<sup>22</sup> with 1 equiv of [Cu(TMPA)(CH<sub>3</sub>CN)]-PF<sub>6</sub><sup>23</sup> (TMPA = tris(2-pyridylmethyl)amine), Scheme 1, yielded an orange CH<sub>2</sub>Cl<sub>2</sub> solution from which complex 1 was isolated as a brown powder, yielding orange crystals by slow diffusion of hexanes.

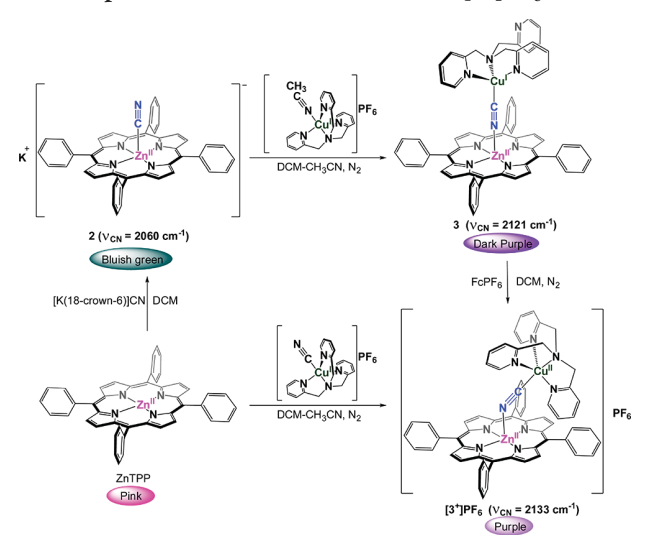
The orientations of the Fe-CN-Cu bridges indicated in Scheme 1 are according to the X-ray diffraction analysis, *vide infra*. Upon oxidation of 1 with 1 equiv of  $Fc^+PF_6^-$ , the color of the solution turned brown, indicating the formation of

Scheme 1. Synthesis of the Cyanide-Bridged [FeFe]-CN-Cu Complex 1 and Its Oxidation Product [1<sup>+</sup>]PF<sub>6</sub><sup>a</sup>



"The orientation of the  $Fe^I$ -CN-Cu $^I$  and  $Fe^I$ -CN-Cu $^I$  is derived from XRD analysis; see text.

Scheme 2. Synthesis of the Cyanide-Bridged (TPP)Zn-CN-Cu Complex 3 and Its Oxidation Product [3<sup>+</sup>]PF<sub>6</sub>



[1<sup>+</sup>]PF<sub>6</sub>, which was isolated as a dark brown solid. Addition of 1 equiv of cobaltocene,  $Cp_2Co$ , returned [1<sup>+</sup>]PF<sub>6</sub> to complex 1.

Via an alternate route, oxidative (Me<sub>3</sub>NO) removal of a carbonyl from  $(\mu\text{-pdt})\text{Fe}_2(\text{CO})_6^{\,24}$  in CH<sub>3</sub>CN solution results in the formation of an intermediate species expected to be either  $(\mu\text{-pdt})\text{Fe}_2(\text{CO})_5(\text{CH}_3\text{CN})$  or  $(\mu\text{-pdt})\text{Fe}_2(\text{CO})_5(\text{NMe}_3)^{.25}$  To this species, addition of [Cu(TMPA)(CN)]-PF<sub>6</sub> $^{23}$  led to the formation of a species of identical spectral properties and, from XRD analysis, identical CN orientation to [1<sup>+</sup>]PF<sub>6</sub>. This result signals a cyanide flip during the linkage process.

The FTIR spectra of 1 and [1<sup>+</sup>]PF<sub>6</sub> (Figure S1) display four carbonyl bands in the 1900–2050 cm<sup>-1</sup> region with bands at 2108 cm<sup>-1</sup> (for 1) and 2112 cm<sup>-1</sup> (for [1<sup>+</sup>]PF<sub>6</sub>) attributed to the bridging cyanide group. The formation of the CN-bridged species 1, from Na[( $\mu$ -pdt)Fe<sub>2</sub>(CO)<sub>5</sub>CN],<sup>22</sup> leads to an increase in the value of  $\nu_{\rm CN}$  from 2093 to 2108 cm<sup>-1</sup>, attributable to kinematic effects.<sup>26,27</sup> On oxidation of 1 to [1<sup>+</sup>]PF<sub>6</sub>, a further minor increase of  $\nu_{\rm CN}$  to 2112 cm<sup>-1</sup> is likely a result of the dipole moment increase from the interaction of Cu<sup>II</sup> vs Cu<sup>I.26</sup>

In order to explore a definite harder metal center for copper—cyanide connection, to ensure that the oxidation of 1 to [1<sup>+</sup>] is localized to the Cu center, and as a reference for the computational studies, *vide infra*, we switched out the [FeFe] portion by (TPP)Zn<sup>2+</sup> (H<sub>2</sub>TPP = 5,10,15,20-tetraphenylporphyrin). This study is similar to that of Holm et al., <sup>16–20</sup> using Zn<sup>II</sup> instead of Fe<sup>II</sup> in the porphyrin side of the adduct. Scheme 2 describes the synthetic approach to the two cyanide-bridged complexes with the Zn-( $\mu$ -CN)-Cu<sup>I/II</sup> linkage, specifically, 3 and [3<sup>+</sup>]PF<sub>6</sub>, which are analogous to complexes 1 and [1<sup>+</sup>]PF<sub>6</sub>.

Complex 2 was obtained following a procedure similar to that reported for  $[K(2,2,2\text{-crypt})][Zn(TPP)(CN)],^{28}$  in our case, using the [K(18-crown-6)] cation. On treating a  $\text{CH}_2\text{Cl}_2$  solution of 2 (blue-green in color) with 1 equiv of  $[\text{Cu}(\text{TMPA})(\text{CH}_3\text{CN})]\text{PF}_6^{\ 23}$  (yellow  $\text{CH}_3\text{CN}$  solution), an immediate color change to dark purple was observed. The concomitant increase of  $\nu_{\text{CN}}$  from 2060  $\text{cm}^{-1}$  in 2 to 2121  $\text{cm}^{-1}$  indicated formation of 3. The orientation of the cyanide bridges in 3 and  $[3^+]$  are deduced from the X-ray diffraction (XRD) analysis, vide infra. Note that the orientation of the cyanide group in 3 is opposite that in the precursor complex 2. Access to the flipped cyanide in this case is likely due to cyanide dissociation from the Zn-CN and capture by the  $\text{Cu}^{\text{I}}$  preceding the formation of the Zn-N-C-Cu I bridge.

Scheme 2 also indicates that oxidation of complex 3 with 1 equiv of  $FcPF_6$ , results in a color change from dark to lighter purple on formation of  $[3^+]PF_6$ . The  $\nu_{CN}$  shifted to a higher value (2133 cm<sup>-1</sup> for  $[3^+]PF_6$ ; Figure S2) attributed to the interaction with the more Lewis acidic  $Cu^{II}$  and the decrease of back-donation from  $Cu^{II}$ . Unlike the results in Scheme 1, the alternative route to generate  $[3^+]PF_6$  starting from  $Zn(TPP)^{29}$  and  $[Cu(TMPA)(CN)]PF_6^{\ 20}$  did not lead to cyanide flipping. The Zn-N-C- $Cu^{II}$  arrangement is expected given the hard nature of the  $Zn^{II}$  receiver. X-ray diffraction analyses of crystals obtained from both pathways reveal the same cyanide orientation. The question of whether cyanide ligand dissociation and free cyanide account for the direction of the cyanide bridge was addressed by isotope labeling experiments:

- (1) A slight excess of <sup>13</sup>CN-labeled [K(18-crown-6)]<sup>13</sup>CN was added to a CH<sub>2</sub>Cl<sub>2</sub> solution of **2** at room temperature. Within the time of mixing, the FTIR spectrum of the resulting solution (Figure S3) revealed the presence of four bands corresponding to **2** [Zn(TPP)CN, 2060 cm<sup>-1</sup>], **2**<sup>#</sup> [Zn(TPP)<sup>13</sup>CN, 2017 cm<sup>-1</sup>], [K(18-crown-6)]CN (2075 cm<sup>-1</sup>), and [K(18-crown-6)]<sup>13</sup>CN (2031 cm<sup>-1</sup>). This rapid exchange confirms the lability of the Zn–CN bond in **2** and the presence of free cyanide.
- (2) <sup>13</sup>CN-labeled Cu<sup>1</sup>(TMPA)(<sup>13</sup>CN) was added to the intact bimetallic complex 3 (1:1) in CH<sub>3</sub>CN with FTIR spectral changes (Figure S4) occurring over the course of an hour and no further changes overnight. Four

distinct bands in the cyanide stretching region were identified as 3 ((TPP)Zn– $N^{12}$ C– $Cu^{I}$ TMPA, 2121 cm<sup>-1</sup>), 3<sup>#</sup> ((TPP)Zn– $N^{13}$ C– $Cu^{I}$ TMPA, 2076 cm<sup>-1</sup>), Cu<sup>I</sup>(TMPA)( $^{13}$ CN) (2051 cm<sup>-1</sup>), and Cu<sup>I</sup>(TMPA)-(CN) (2095 cm<sup>-1</sup>), which were prepared separately (see Experimental Section for details).

The slower exchange of the Cu(TMPA)(CN) metalloligand bound to the ZnTPP unit with the labeled  $Cu(TMPA)(^{13}CN)$  (in comparison to the [(TPP)ZnCN/free CN- exchange) points toward the fact that in solution complex 3 is in equilibrium with dissociated components, Zn(TPP) and Cu(TMPA)(CN), as shown in Scheme 3, consistent with

Scheme 3. Equilibrium between Complex 3, Zn(TPP), and Cu(TMPA)(CN) in  $CH_2Cl_2$  Solution

the computational results, vide infra. It should be noted that the FTIR spectrum of 3 in  $CH_2Cl_2$  solution shows its presence as the major component (ca. 80%), with a shoulder at 2095 cm<sup>-1</sup> corresponding to Cu(TMPA)(CN) (ca. 20%, Figure S2) suggesting the equilibrium in Scheme 3 lies mostly toward the left. These experimental labeling studies imply that the Zn-axial ligand in Zn(TPP) is labile, whereas the Cu-CN bond is stable, regardless of the oxidation state of Cu. The DFT computational results below are consistent with this conclusion.

**X-ray Diffraction Analysis.** Complex 1 crystallizes in the orthorhombic crystal system,  $P2_12_12_1$  space group, while  $[1^+]PF_6$  is in the monoclinic, P121/c1 space group (see Figures 2, S5, and S6). The Cu centers in both the complexes are in trigonal bipyramidal geometry with the three pyridyl-N donors in the trigonal plane. The metric data (Table 1) for the [FeFe] part of 1 are fairly close to those of a similar cyanide-bridged complex, FeFe-CN-Fe', where  $Fe' = [(\eta^5-C_5H_5)-Fe^{II}(CO)_2]^{+11}$ 

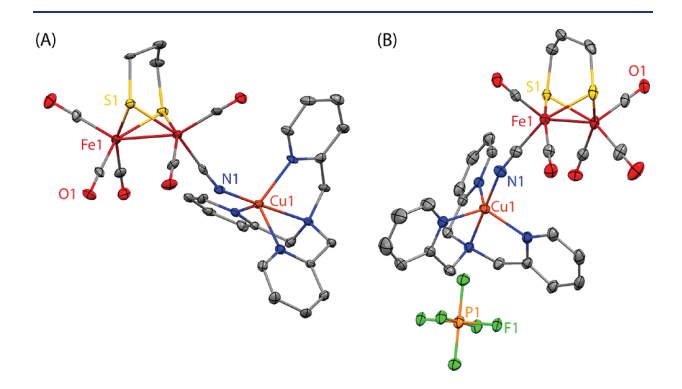


Figure 2. Perspective views as thermal ellipsoids, 50% probability level, of (A) 1 and (B)  $[1^+]PF_6$  from X-ray diffraction analysis. (H atoms and solvent molecules have been omitted for clarity.)

Table 1. Selected Metric Data

(FeFe-CN-Cu)	$Fe-C(N)^a$	C-N <sup>a</sup>	$Cu-N(C)^a$	Fe-C-N <sup>b</sup>	$Cu-N-C^b$	Fe-Fe <sup>a</sup>	$Cu-N_{ax(TMPA)}^{a}$	$\text{Cu-N}_{\text{eq(TMPA)}}^{i}$	ref
1	1.90(1)	1.17(1)	1.992(9)	176.9(9)	155.2(8)	2.514(2)	2.456(8)	2.091(9)	this work
$[1^+]PF_6$	1.904(6)	1.129(7)	1.947(5)	176.8(5)	164.0(5)	2.5176(11)	2.024(4)	2.063(4)	this work
FeFe-CN-Fe'c	1.917(4)	1.152(4)	$1.930(3)^d$	177.2(3)	$177.6(2)^e$	2.5221(7)			11
(Zn-NC-Cu)	Zn-N	$Zn-N(C)^a$		$Cu-C(N)^a$		$Zn-N-C^b$	Cu-C-N <sup>b</sup>	$\Delta^{\operatorname{Zn}}_{24}^{f}$	ref
3	2.050	2.050(3)		1.878(4	)	172.8(3)	173.3(3)	0.446	this work
$[3^+]PF_6$	2.104	2.104(6)		1.940(8	)	152.7(5)	178.0(6)	0.400	this work
$[Zn(TPP)(CN)]^{-}$ 2.174(2) <sup>g</sup>		1.148(3)			$175.36(21)^h$		0.5821(5)	28	

"Distance in Å. hAngle in deg. (μ-pdt)Fe<sub>2</sub>(CO)<sub>5</sub>CN-Fe(CO)<sub>2</sub>(η<sup>5</sup>-C<sub>5</sub>H<sub>5</sub>). Fe-N(C) bond distance. Fe'-N-C bond angle. Displacement of zinc from the least-squares plane of the C<sub>20</sub>N<sub>4</sub> porphyrinato core. <sup>g</sup>Zn-C(N) bond distance. <sup>h</sup>Zn-C-N bond angle. <sup>i</sup>Average distance in Å.

Upon oxidation of 1, the [FeFe] unit remains unaltered, while significant metric changes can be observed for the Cu(TMPA) unit, indicating that the oxidation has taken place at the Cu center. The decrease in Cu-N(C) bond distance from 1.992(9) Å to 1.947(5) Å on going from 1 to  $[1^+]PF_6$  is consistent with the increase in oxidation state of Cu. The Cu- $N_{ax}(TMPA)$  distance shrinks from 2.456(8) Å in 1 to 2.024(4) Å in  $[1^+]PF_6$ ; the average  $Cu-N_{eq}(TMPA)$  distance also shortens on going from 1, 2.090(9) Å, to [1+]PF<sub>6</sub>, 2.063(4) Å. The Cu-N-C angle increases upon oxidation from 155.2(8)° in 1 to  $164.0(5)^{\circ}$  in  $[1^{+}]PF_{6}$ , presumably to minimize steric interaction as the [FeFe]...Cu distance (nonbonding distance of the Cu from the closest Fe of the [FeFe] unit) decreases from 4.939(2) Å in 1 to 4.920(1) Å in  $[1^+]PF_6$ .

Complexes 3 and [3<sup>+</sup>]PF<sup>6</sup> crystallize in monoclinic crystal systems with P121/n1 and P121/c1 space groups, respectively (see Figures 3, S7, and S8). The orientation of the cyanide

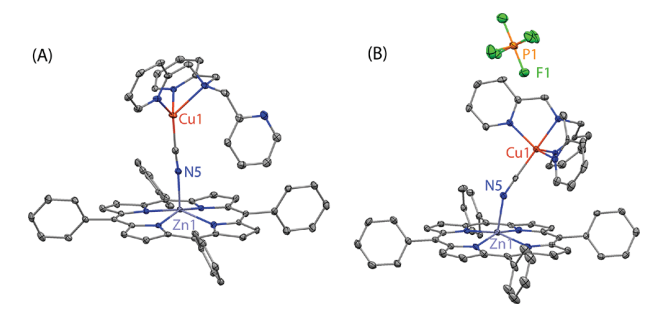


Figure 3. Perspective views as thermal ellipsoids, 50% probability level, of (A) 3 and (B) [3<sup>+</sup>]PF<sub>6</sub> from X-ray diffraction analysis. (H atoms and solvent molecules have been omitted for clarity.)

(Cu-CN-Zn vs Cu-NC-Zn, for example) in 3 and [3+]PF<sub>6</sub> has been assigned based on XRD refinements, a common practice for such organometallic complexes. 11,14,17,20,30 Upon exchanging the C45 and N5 atoms (the carbon and nitrogen atoms of the bridging cyanide group) and subsequent refinement, the thermal ellipsoids of C45 and N5 were respectively rendered nonpositive definite and significantly elongated (Figures S9 and S10), suggesting a wrong assignment. Note that the Cu<sup>1</sup> center in 3 assumes a distorted tetrahedral geometry with one unbound pyridyl group hanging off the TMPA ligand, while the Cu<sup>I</sup> center in 1 prefers pentacoordination in trigonal bipyramidal (TBP) geometry. Upon oxidation, the Cu<sup>II</sup> center in 3 switches into TBP pentacoordination, similarly to 1<sup>+</sup>, which retains TBP geometry.

Electrochemistry. Figure 4 shows the cyclic voltammograms of complexes 1 (in CH<sub>3</sub>CN) and 3 (in CH<sub>2</sub>Cl<sub>2</sub>). For 1, the  $Cu^{II/I}$  redox couple appears as a reversible event with  $E_{1/2}$  =

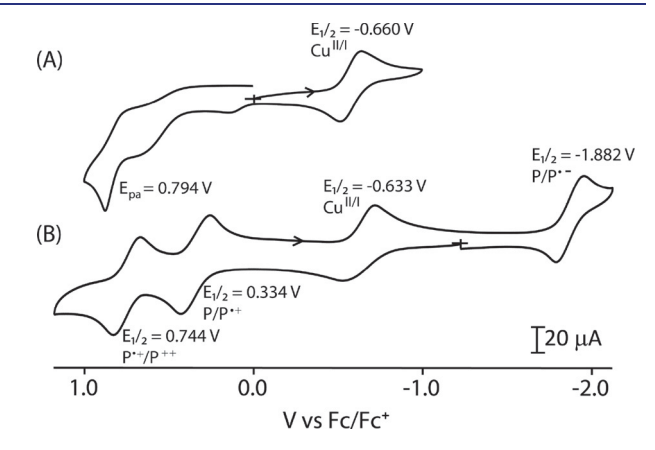


Figure 4. Cyclic voltammograms, under Ar, of 2.0 mM solutions of (A) 1 (in CH<sub>3</sub>CN) and (B) 3 (in CH<sub>2</sub>Cl<sub>2</sub>) containing 0.1 M  $[{}^tBu_4N][PF_6]$  as supporting electrolyte and 200 mV s $^{-1}$  scan rate. The arrow indicates the direction of scan.

-0.660 V. The scan rate dependence of this couple (Figure S11) further supports its reversibility. An irreversible anodic event at 0.794 V is attributed to the oxidation of the diiron center. Complex 3 shows four reversible redox events in the 1.2 V to -2.0 V range. The event at  $E_{1/2} = -0.633$  V is assigned to the Cu<sup>II/I</sup> redox couple, and the events at  $E_{1/2} =$ 0.334, 0.744, and -1.882 V correspond to the porphyrin ringcentered redox events. At 0.334 V the porphyrin ring loses one electron to generate a porphyrin  $\pi$ -cation radical  $(P^{\bullet+})$  and a second electron is removed at a higher potential (0.744 V), leading to the formation of a porphyrin dication  $(P^{2+})$ . However, at much more negative potential (-1.882 V) an electron is added to the porphyrin ring, resulting in a porphyrin  $\pi$ -anion radical ( $P^{\bullet-}$ ). Figures S12 and S13 show the scan rate dependence and multiple scans, respectively, of the redox couples of 3, further supporting the reversible nature of these events and also implying that no chemical transformations take place in the process.

**Electron Paramagnetic Resonance Spectroscopy.** The X-band EPR spectra of frozen CH<sub>3</sub>CN ([1<sup>+</sup>]PF<sub>6</sub>) and CH<sub>2</sub>Cl<sub>2</sub> ([3+]PF<sub>6</sub>) solutions of the copper(II) complexes, at 3.6 K, showed the presence of a single paramagnetic,  $S = \frac{1}{2}$ , species with hyperfine lines corresponding to the coupling of the unpaired electron with the Cu-63 and Cu-65 nuclei, both of which have  $I = \frac{3}{2}$ . No superhyperfine splitting resulting from coupling with the nitrogen atoms of the TMPA or the bridging CN was detected (Figure 5) possibly due to line-broadening effects. Table S1 lists the g values and the hyperfine coupling constants, A, obtained by simulation of the EPR spectra. Both complexes display a pseudoaxial EPR signal ( $[1^+]$ PF<sub>6</sub>:  $g_1 =$ 

Journal of the American Chemical Society

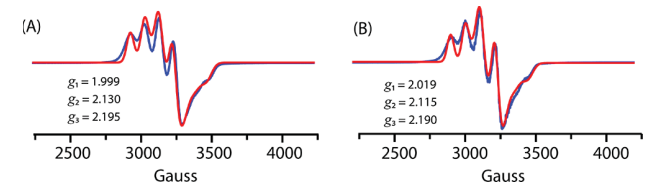


Figure 5. EPR spectrum of (A) frozen  $CH_3CN$  solution of  $[1^+]PF_6$  and (B) frozen  $CH_2Cl_2$  solution of  $[3^+]PF_6$  at 3.6 K. The blue trace is the experimental spectrum, and the red trace is the simulated spectra (doublet).

1.999,  $g_2 = 2.130$ , and  $g_3 = 2.195$ ;  $[3^+]PF_6$ :  $g_1 = 2.019$ ,  $g_2 = 2.115$ , and  $g_3 = 2.190$ ) with well-resolved hyperfine splitting, resulting in R values,  $(g_2 - g_1)/(g_3 - g_2)$ ,  $^{31}$  equal to 2.015 for  $[1^+]PF_6$  and 1.28 for  $[3^+]PF_6$ . These values,  $g_1 < 2.04$  and R > 1, along with the values of the hyperfine splitting parameters, indicate the population of a  $d_z^2$  ground state, a characteristic of trigonal bipyramidal geometries.  $^{32,33}$  Therefore, we assert that the solid state structure, as observed from XRD where the Cu(II) has a trigonal bipyramidal geometry, is retained in solution for both complexes  $[1^+]PF_6$  and  $[3^+]PF_6$ .

**Computational Studies.** DFT calculations were applied to investigate the isomers and transition states in the bridging cyanide isomerization in 1 and 3. The structures of 1,  $1^+$  (from  $[1^+]PF_6$ ), 3, and  $3^+$  (from  $[3^+]PF_6$ ) from XRD were used as initial geometric references in these calculations. To reduce computational cost, the phenyl in TPP in 3 was replaced by hydrogen. The structural models and corresponding energetics were obtained by the B3LYP functional. Hore details about the methodology can be found in the Experimental Section. The calculated geometries for all species are listed in the SI. Note: The designation Cu\* indicates the absence of one axial aminyl  $N_{\rm ax}({\rm TMPA})$ –Cu bond.

Isomers of 1/1<sup>+</sup> and Their Structures. The complexes 1 (FeFe-CN-Cu\*) and 1+ ([FeFe-CN-Cu]+) were determined by X-ray diffraction to have an FeFe-CN-Cu sequence, regardless of their synthetic precursors. The oxidation of 1 to 1+ is assigned to the CuI/II redox couple by the computational spin densities. In 1, the copper is de facto four-coordinate with a long axial aminyl N<sub>av</sub>(TMPA)-Cu distance (2.612 Å, calcd/2.456 Å, exptl) and an electron count of 18-e (Cu $^{\! \rm I}$  ). Upon oxidation, the  $N_{ax}-Cu$  distance decreases to 2.154 Å (calcd)/2.024 Å (exptl). The newly established N<sub>ax</sub>-Cu bond and the change of the coordinating atom of cyanide from C to N creates a five-coordinate, electron-rich Cu<sup>II</sup> (19-e). The linkage cyanide isomers of 1 and 1<sup>+</sup> were evaluated, finding that [FeFe-CN-Cu\*] (1) and [FeFe-CN-Cu]<sup>+</sup> (1<sup>+</sup>) are more stable than their isomers [FeFe-NC-Cu\*] (1') and [FeFe-NC-Cu\*]+ (1') by 5.2 and 18.3 kcal/mol, respectively. Therefore, the computations confirm no linkage cyanide isomerization is to be expected during the oxidation of 1 to 1<sup>+</sup>.

The large Gibbs free energy difference between linkage isomers  $\mathbf{1}^+$  and  $\mathbf{1}'^+$  is related to their electronic structures. A breakdown of the difference (Table S2) shows the primary contribution is from the solvation correction, which depends on the electron distributions. The electrostatic potential plots (Figure 6, trace 1) show  $\mathbf{1}'^+$  is less polarized, and thus it receives less solvation stabilization.

The [FeFe-NC-Cu\*]+, or 1'+, is expected to be the immediate product on combining [Cu(TMPA)(CN)]+ ([Cu-CN]+) and  $(\mu$ -pdt)[Fe(CO)<sub>3</sub>][Fe(CO)<sub>2</sub>()], where () repre-

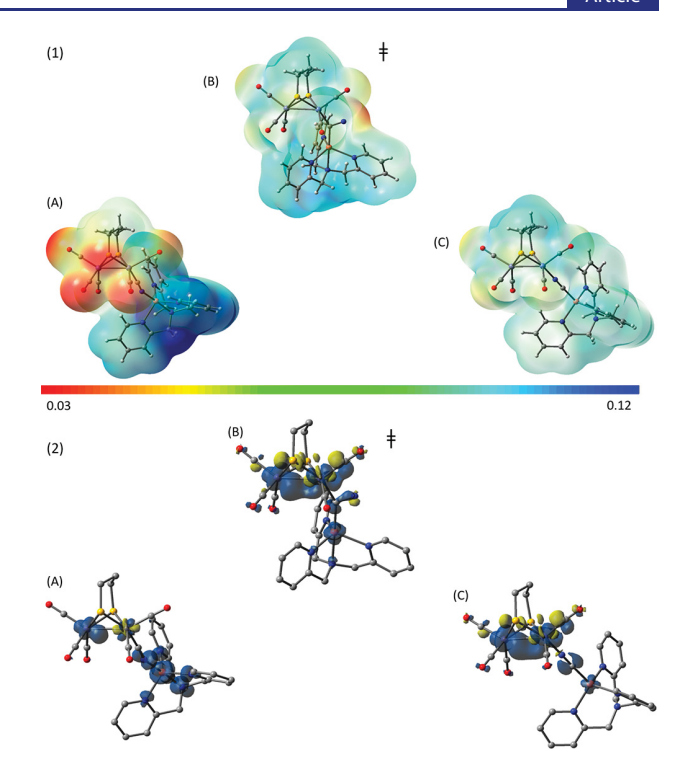


**Figure 6.** Electrostatic potential plots (1) and spin densities (2, values in parentheses) of (A) [FeFe-CN-Cu] $^+$  ( $1^+$ , Fe $_{left}$  0.29, Fe $_{right}$  -0.02, Cu 0.49), (B) the transition state connecting the linkage isomers (Fe $_{left}$  0.66, Fe $_{right}$  0.19, Cu 0.17), and (C) [FeFe-NC-Cu\*] $^+$  ( $1'^+$ , Fe $_{left}$  0.54, Fe $_{right}$  0.64, Cu 0.03).

sents the open site, Figure 7. Computations find that the adduct is formed with only a mild energy hike (1.9 kcal/mol). However, the spin densities of 1'+ revealed an oxidation state assignment of Fe<sup>1.5</sup>Fe<sup>1.5</sup>Cu<sup>I</sup>, which is not inherited from its precursors, namely, Fe<sup>I</sup>Fe<sup>I</sup>Cu<sup>II</sup>; thus a charge transfer is

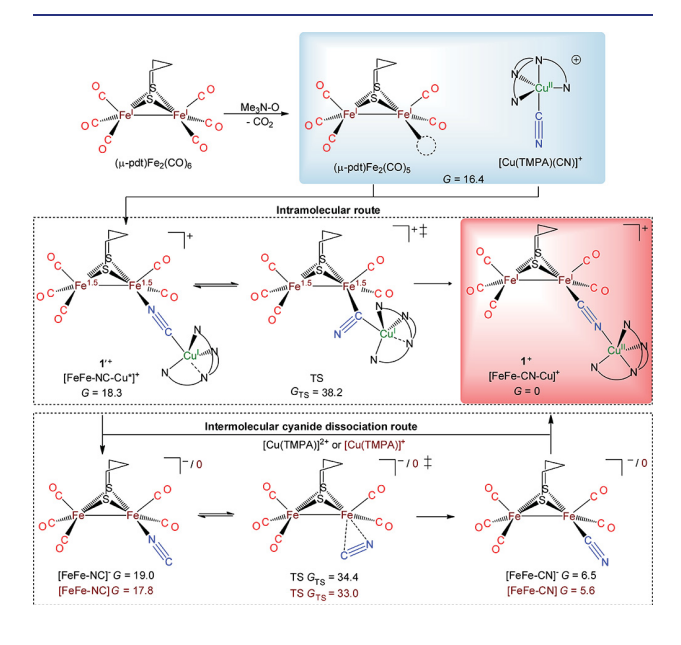


Figure 7. Computational mechanism for the production of  $\mathbf{1}^+$  requires either intermolecular or intramolecular linkage cyanide isomerization in order to establish the experimentally observed sequence of FeFe-C-N-Cu.

concomitant with its formation. The establishment of the Fe-N<sub>CN</sub> bond in 1'+ pushes one electron out of the bonding orbital of the diiron unit to the copper unit, which responds by cleaving the N<sub>ax</sub>-Cu bond, rendering a four-coordinate 18-e Cu(I). In this case, the copper can flexibly act as an electron reservoir to accept the electron as it concomitantly breaks the Cu-N<sub>ax</sub> bond and accommodates the incoming electron.

Cyanide Flipping Mechanism between 1'+ and 1+. A linkage cyanide flipping is necessary to convert the intermediate 1'+ into 1+. Our previous work discussed the possible bridging cyanide isomerization mechanism(s) of a series of FeFe-CN/NC-Fe tri-iron complexes. 11 In that scenario, relatively strong bonds exist between Fe and C or N of the cyanide, and thus the dissociation of cyanide and recombination with flipping is not feasible. The intramolecular mechanism, featuring a  $\mu_2$ -carbon in the transition state, still has relatively high barriers (>30 kcal/mol) that prevent the thermodynamically favored isomerization, even though such intramolecular flipping does not require complete rupture of Fe-C and/or Fe-N bonds.

The isomer 1'+ is 18.3 kcal/mol higher than 1+ in Gibbs free energy due to its unfavorable solvation and makes the isomerization thermodynamically possible. The intramolecular transition state between  $\mathbf{1}'^+$  into  $\mathbf{1}^+$  likewise features a  $\mu_2$ carbon connection to both FeFe and Cu fragments. The transition state (G = 38.2 kcal/mol) has an oxidation state, Fe<sup>1.5</sup>Fe<sup>1.5</sup>Cu<sup>I</sup>, close to 1'+, thus is not well solvated, rendering a net rate-determining Gibbs free energy barrier of 21.8 kcal/mol with respect to the precursors, Figure 7.

Intermolecular isomerization mechanisms were explored as well. The intermediate  $\mathbf{1}'^+$  may dissociate into ion pairs, either  $[FeFe-NC]^{-}[Cu(TMPA)]^{2+}$  or  $[FeFe-NC]^{0}[Cu(TMPA)]^{+}$ , where the cyanide flipping might occur on the [FeFe-CN]<sup>+/0</sup> fragment. The transition state Gibbs free energies are similar for two oxidation states of [FeFe-CN], 34.4 and 33.0 kcal/mol, with net barriers of 18.0 and 16.6 kcal/mol, respectively. They are actually more accessible than the above-mentioned intramolecular barrier. It is notable that the close energetics of these two routes reflect that the [FeFe-NC]<sup>0/-1</sup> and  $[Cu(TMPA)]^{2+/+} \ \ fragments \ \ have \ \ similar \ \ redox \ \ potentials$ and validate the intramolecular charge transfer. After the experimentally required cyanide flipping and the generation of 1<sup>+</sup>, more likely via an intermolecular path, the carbon end of the cyanide, with a demand to establish good back-bonding on the diiron unit, reclaims the electron from the copper unit with the Cu-N<sub>av</sub> reinstated in a reverse electron transfer. This concludes the copper fragment's role as the electron reservoir. The unpaired electron of  $1^+$  primarily resides on Cu's  $d_z^2$ orbital, consistent with EPR evidence.

The electron transfer in 1'+ and its resultant electronic structure, subject to poor solvation, facilitate the linkage cyanide flipping process thermodynamically and probably kinetically as well. A similar intramolecular isomerization between 1 (G = 0) and 1' (G = 5.2) incurs a smaller Gibbs free energy difference and a relatively high barrier ( $G_{TS} = 30.6 \text{ kcal/}$ mol), as the Cu<sup>I</sup> unit is already saturated, and thus no charge transfer or variations in solvation stabilization are observed to facilitate the linkage cyanide isomerization.

Isomerization of Complex 3. Isomers of 3 and 3<sup>+</sup>. Complex 3<sup>\$</sup> (i.e., experimental product 3, the designation \$ indicates the absence of an equatorial pyridinyl N<sub>eq</sub>-Cu bond), synthesized from two precursors, [Zn(TPP)(CN)]  $(2^-)$  and  $[Cu(TMPA)(NCCH_3)]^+$  ( $[Cu^*-NCCH_3]^+$ ), fea-

tures a Zn-N-C-Cu sequence, with a flipped linkage cyanide, compared to the CN orientation in its precursor. In addition to the swap of the coordination atom to the cyanide, the copper unit also loses one equatorial pyridinyl, N<sub>eq</sub>, from TMPA, rendering a distorted tetrahedral coordination environment around Cu<sup>1</sup> in 3<sup>\$</sup>. This contrasts with the loss of the N<sub>ax</sub>-Cu<sup>1</sup> bond in 1. Four isomers of 3<sup>\$</sup> were computationally evaluated: Zn-NC-Cu\$ (3\$), Zn-CN-Cu\$ (3\$'), Zn-NC-Cu\* (3\*), and Zn-CN-Cu\* (3\*'). The complex  $3^{\$}$ , subject to X-ray diffraction, is computationally confirmed to be the most stable isomer (Table S3). Apparently,  $Cu^{I}(d^{10})$  prefers  $\pi$ -acceptor(s) over  $\sigma$ -donors such that the cyanide flipping is justified during its synthesis. The N<sub>eq</sub>-Cu bond in the isomer 3\* may be reinstated at the cost of the rupture of the N<sub>ax</sub>-Cu bond; therefore the coordination number around Cu<sup>I</sup> remains four in all isomers of 3\$ to avoid the overcrowding of electrons. It is noteworthy to mention that Zn has an electron count of 20 in 3<sup>\$</sup> and all other isomers. The calculations predict dissociation of 3\$ into Zn(porphyrin) and Cu(TMPA)(CN) (Cu\$-CN) by -12.7 kcal/mol. The lability of the Zn–NC bond on 3<sup>\$</sup> (i.e., 3in the Experimental Section) was confirmed by the isotopelabeled ligand exchange as monitored by IR, vide infra. However, the dissociation of the Cu-C bond of 3\$\\$ is calculated to be unfavored by 8.0 kcal/mol.

Complex 3<sup>+</sup>, synthesized by oxidizing complex 3<sup>\$</sup>, inherits the Zn-N-C-Cu sequence. The major structural difference is that the previously ruptured N<sub>eq</sub>-Cu bond is regenerated, while all N<sub>ax</sub>-Cu bonds are preserved. The axial aminyl N<sub>ax</sub> is predicted to be closer to Cu in  $3^+$  (2.216 Å calcd/2.033 Å exptl) in comparison to the N<sub>ax</sub>-Cu bond in the comparable isomer 3\* (2.618 Å calcd). The energetic data also confirm it is the most stable isomer (Table S3); therefore, no cyanide linkage isomerization is expected during the oxidation of 3\$ to 3<sup>+</sup>. Similar to 3<sup>\$</sup>, the dissociation of the Zn-N bond in 3<sup>+</sup> gains an advantage of -12.1 kcal/mol in Gibbs free energy.

Cyanide Linkage Isomerization Mechanism of 35. Compared to the previous FeFe-Cu case discussed, the signature property of 3<sup>\$</sup> and its isomers is that both metalcyanide bonds are expected to be weak, with already saturated metals: Cu<sup>I</sup>(d<sup>10</sup>), if coordinated by four nitrogen atoms of TMPA, and Zn<sup>II</sup>(d<sup>10</sup>) if coordinated by four nitrogen atoms of porphyrin. The systems gain a total advantage of 15.5 kcal/mol in Gibbs free energy for both precursors of 3<sup>8</sup> to dump one ligand: the cyanide for [Zn(porphyrin)CN] and the acetonitrile for [Cu(TMPA)(NCCH<sub>3</sub>)]<sup>+</sup>, Figure 8. The dissociated cyanide, specifically its carbon atom, is then captured by the Cu fragment, which is also a favored process by  $\Delta G = -3.3$  kcal/mol. The resultant electron crowding instigates the dissociation of one equatorial  $N_{\text{eq}}$  and leaves the four-coordinate Cu(TMPA)(CN) fragment with one dangling pyridinyl nitrogen from TMPA. However, it is predicted to take  $\Delta G = 12.7$  kcal/mol to attach the nitrogen end of the cyanide on Cu\$-CN to Zn(porphyrin) to generate 3\$, whose existence is crystallographically confirmed. The labeling experiment (vide supra), Scheme 3, further shows evidence of the N-Zn bond cleavage and supports the intermolecular

The intramolecular cyanide flipping mechanism, resembling the one for the FeFe-Cu systems, is made possible by generating the intermediate 3\*', Figure 8. One equatorial  $N_{eq}$ is cleaved before the formation of the transition state featuring a  $\mu_2$ -C to flip the linkage cyanide, creating the other intermediate  $3^{\$'}$ . This mechanism is relatively unfavored with

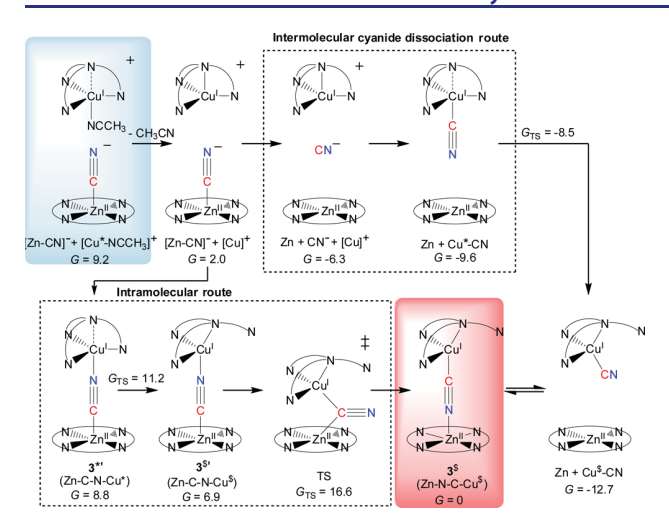


**Figure 8.** Possible mechanisms involved in the formation of complex 3<sup>\$</sup>. Implicit solvation of acetonitrile by the SMD model was added. Note: there is an explicit acetonitrile with Cu\*-NCCH<sub>3</sub><sup>+</sup>.

higher transition state Gibbs energy due to the weak metal—cyanide bond energies that are overcome by an entropy penalty, failing to firmly hold these components together, Figure 8.

Overview of the Cyanide Isomerization Mechanism. The DFT studies of mechanisms for linkage cyanide isomerizations or flips in FeFe-CN-Cu and Zn-NC-Cu, in addition to our two other studies concerning tri-iron systems and Holm's Fe-Cu systems,<sup>35</sup> provide a platform to generalize the conditions that will lead to bridging cyanide flipping: (1) The initial geometry of the bridging cyanide-containing complex, as predetermined by the precursors, must be unfavorable. (2) There must be a difference of properties of metals on both ends. (3) There should be a mismatch of ligand—metal preference. This is the thermodynamic prerequisite of the cyanide linkage isomerization.

To further make the isomerization possible, the barrier must be accessible, through either an intramolecular or intermolecular mechanism. This is the kinetic prerequisite. Unlike Holm's system, which prefers an intramolecular mechanism, the two cases presented here are examples where intermolecular mechanisms are more favored. Weak cyanide-metal bonds would help the dissociation of the cyanide as a free ion so that it can freely reorganize its structure; this is applicable to the Zn-NC-Cu case. For the FeFe-CN-Cu case, the strong bonds are present in the first place but their dissociations are compensated by the variation of the solvation level, rendering a relatively low bond dissociation energy. The intermolecular cyanide flipping depends on the ease of such bond dissociations. The dilemma is, if the bonds are just too weak, it is no longer possible to maintain a stable bridging cyanide and an equilibrium between the associated and dissociated M-N bond may arise as a result.

The intramolecular isomerization is somewhat a compromise in situations where bonds are too strong to dissociate, as the  $\mu_2$ -carbon transition state does not require complete rupture of the relevant bonds. The barrier may not be easily accessible though, as reflected by our earlier study of the triiron system, <sup>11</sup> unless the electronic structure can be tuned to reduce the gap between the intermediate and the transition state. The iron, coordinated by porphyrin in Holm's Fe-Cu

systems, <sup>17,20</sup> is able to perform spin crossover, thus stabilizing the transition state and making possible the intramolecular isomerization.<sup>35</sup>

#### CONCLUDING REMARKS

The salient conclusions from this study follow. Cyanide-bridged complexes with [FeFe]-CN-Cu<sup>1/II</sup> and Zn-NC-Cu<sup>1/II</sup> platforms demonstrate a cyanide flip upon adduct formation that may be induced in both, depending on the choice of cyanide-containing precursor. The ultimate orientation of cyanide ligand in these complexes is consistent with the fact that the soft carbon end of the cyanide prefers to bind the softer metal, while the nitrogen end binds to the harder metal center. A second effect is the shift in electrostatic potential that leads to solvation differences, reinforcing the FeFe-CN-Cu favored arrangement in the case of 1.

The hard, but electron-saturated, Zn<sup>II</sup> center makes the cyanide flip more feasible in the Zn-NC-Cu complexes which were found, by experiment and by computation, to be in equilibrium with free Zn(TPP) and the Cu(TMPA)CN fragments. The Zn-N<sup>12</sup>C-Cu<sup>I</sup> exhibited NC-Cu<sup>I</sup> metalloligand exchange in the presence of N<sup>13</sup>C-Cu<sup>I</sup> to give both Zn-N<sup>12</sup>C-Cu<sup>I</sup> and Zn-N<sup>13</sup>C-Cu<sup>I</sup>. However, in the crystalline solid only Zn-NC-Cu units are observed; FTIR spectroscopy in CH<sub>2</sub>Cl<sub>2</sub> solution indicates an approximate 4:1 ratio of the intact bimetallic to its monometallic components.

Detailed computational investigations into the cyanide flipping mechanism revealed that an intermolecular or dissociative mechanism involving cleavage of at least one metal cyanide bond is more energetically favorable for both cases, compared to the intramolecular mechanism that maintains some M–M′ connectivity via the cyanide. It also highlights the kinetic and thermodynamic prerequisites of such isomerization processes wherein an accessible energy barrier between the two isomers is essential.

Our study endeavored to illuminate the role of the cyanide ligand and the [4Fe4S] cluster of the apo-HydF enzyme, in assembly and transfer of the [FeFe] subunit during the maturation process. Therefore, the cyanide flip observed when the [4Fe4S] cluster of the apo-HydF binds the synthetic diiron complex during the maturation process, as reported by Berggern et al., is likely influenced by the diiron core as well as the [4Fe4S] cluster. That is, if the major function of HydF turns out to be an in vivo transporter, carrying the diiron unit specifically to the apo-Hyd A, its responsibilities would include both securing the diiron unit during capture and transport and prompt release of the unit at the destination. Such a process requires a flexible and controllable docking/ dedocking mechanism and triggered by alteration of electronic environment. Although the iron centers in the synthetic [FeFe] subunit and the [4Fe4S] cluster have been spectroscopically found to be in +1 and +2.5 redox states, respectively,<sup>5</sup> it is quite uncertain whether a transient charge transfer between the centers occurs during the docking process, which could alter the redox states, as observed in the case of the [FeFe]-CN-Cu complex. We might expect however the iron of the [4Fe4S] cluster that engages in the docking process to be reduced, preferring C-bound cyanide, while the iron of the diiron complex becomes oxidized. If so, both the loss of a carbonyl ligand, Figure 1, and the back flip of the cyanide might be rationalized. Such an attractive proposal is however at this time an interesting supposition. Nevertheless recent studies that suggest cyanoironcarbonyl units are attached to iron-sulfur

clusters in the biosynthesis of [FeFe]-hydrogenase active site would argue for additional model studies that explore the ambidentate character of cyanide under such bioinorganic conditions.<sup>36</sup>

#### ASSOCIATED CONTENT

## Supporting Information

The Supporting Information is available free of charge on the ACS Publications website at DOI: 10.1021/jacs.8b04189.

Experimental procedures; additional spectroscopic, electrochemical, and computational details (PDF)

Crystallographic data for complex 1 (CIF)

Crystallographic data for [1<sup>+</sup>]PF<sub>6</sub> (CIF)

Crystallographic data for 3 (CIF)

Crystallographic data for [3<sup>+</sup>]PF<sub>6</sub> (CIF)

## AUTHOR INFORMATION

#### **Corresponding Authors**

\*hall@science.tamu.edu

\*marcetta@chem.tamu.edu

#### ORCID ®

Donald J. Darensbourg: 0000-0001-9285-4895

Michael B. Hall: 0000-0003-3263-3219

Marcetta Y. Darensbourg: 0000-0002-0070-2075

#### Notes

The authors declare no competing financial interest. Crystallographic data for complexes 1, [1<sup>+</sup>]PF<sub>6</sub>, 3, and [3<sup>+</sup>]PF<sub>6</sub> were deposited in the Cambridge Crystallographic Data Centre. The following CCDC numbers were assigned to them: 1 (CCDC 1835892), [1<sup>+</sup>]PF<sub>6</sub> (CCDC 1835893), 3 (CCDC 1835894), and [3<sup>+</sup>]PF<sub>6</sub> (CCDC 1835895).

# **■** ACKNOWLEDGMENTS

We are grateful for financial support from the National Science Foundation (CHE-1665258 to M.Y.D. and CHE-1664866 to M.B.H.) and the Robert A. Welch Foundation (A-0924 to M.Y.D. and A-0648 to M.B.H.). The authors acknowledge the Laboratory for Molecular Simulation at Texas A&M University for providing computing resources.

#### REFERENCES

- (1) Lubitz, W.; Ogata, H.; Rüdiger, O.; Reijerse, E. Chem. Rev. 2014, 114, 4081–4148.
- (2) Simmonsa, T. R.; Berggren, G.; Bacchi, M.; Fontecave, M.; Artero, V. Coord. Chem. Rev. 2014, 270-271, 127-150.
- (3) Vignais, P. M.; Billoud, B. Chem. Rev. 2007, 107, 4206-4272.
- (4) Fontecilla-Camps, J. C.; Volbeda, A.; Cavazza, C.; Nicolet, Y. Chem. Rev. 2007, 107, 4273-4303.
- (5) Berggren, G.; Adamska, A.; Lambertz, C.; Simmons, T. R.; Esselborn, J.; Atta, M.; Gambarelli, S.; Mouesca, J.-M.; Reijerse, E.; Lubitz, W.; Happe, T.; Artero, V.; Fontecave, M. *Nature* **2013**, 499, 66–70.
- (6) Esselborn, J.; Lambertz, C.; Adamska-Venkatesh, A.; Simmons, T. R.; Berggren, G.; Noth, J.; Siebel, J. F.; Hemschemeier, A.; Artero, V.; Reijerse, E.; Fontecave, M.; Lubitz, W.; Happe, T. *Nat. Chem. Biol.* **2013**, *9*, 607–610.
- (7) Caserta, G.; Pecqueur, L.; Adamska-Venkatesh, A.; Papini, C.; Roy, S.; Artero, V.; Atta, M.; Reijerse, E.; Lubitz, W.; Fontecave, M. *Nat. Chem. Biol.* **2017**, *13*, 779–787.
- (8) Lampret, O.; Adamska-Venkatesh, A.; Konegger, H.; Wittkamp, F.; Apfel, U.-P.; Reijerse, E. J.; Lubitz, W.; Rüdiger, O.; Happe, T.; Winkler, M. J. Am. Chem. Soc. 2017, 139, 18222–18230.

- (9) Adamska-Venkatesh, A.; Roy, S.; Siebel, J. F.; Simmons, T. R.; Fontecave, M.; Artero, V.; Reijerse, E.; Lubitz, W. *J. Am. Chem. Soc.* **2015**, *137*, 12744–12747.
- (10) Esselborn, J.; Muraki, N.; Klein, K.; Engelbrecht, V.; Metzler-Nolte, N.; Apfel, U.-P.; Hofmann, E.; Kurisu, G.; Happe, T. *Chem. Sci.* **2016**, 7, 959–968.
- (11) Lunsford, A. M.; Beto, C. C.; Ding, S.; Erdem, Ö. F.; Wang, N.; Bhuvanesh, N.; Hall, M. B.; Darensbourg, M. Y. *Chem. Sci.* **2016**, *7*, 3710–3719.
- (12) Geiss, A.; Vahrenkamp, H. Inorg. Chem. 2000, 39, 4029-4036.
- (13) Geiss, A.; Kolm, M. J.; Janiak, C.; Vahrenkamp, H. Inorg. Chem. **2000**, 39, 4037–4043.
- (14) Shatruk, M.; Dragulescu-Andrasi, A.; Chambers, K. E.; Stoian, S. A.; Bominaar, E. L.; Achim, C.; Dunbar, K. R. *J. Am. Chem. Soc.* **2007**, *129*, 6104–6116.
- (15) Darensbourg, D. J.; Yoder, J. C.; Holtcamp, M. W.; Klausmeyer, K. K.; Reibenspies, J. H. *Inorg. Chem.* **1996**, *35*, 4764–4769.
- (16) Lee, S. C.; Scott, M. J.; Kauffmann, K.; Münck, E.; Holm, R. H. J. Am. Chem. Soc. 1994, 116, 401–402.
- (17) Scott, M. J.; Holm, R. H. J. Am. Chem. Soc. 1994, 116, 11357–11367.
- (18) Scott, M. J.; Lee, S. C.; Holm, R. H. Inorg. Chem. 1994, 33, 4651-4662.
- (19) Gardner, M. T.; Deinum, G.; Kim, Y.; Babcock, G. T.; Scott, M. J.; Holm, R. H. *Inorg. Chem.* **1996**, *35*, 6878–6884.
- (20) Lim, B. S.; Holm, R. H. Inorg. Chem. 1998, 37, 4898-4908.
- (21) Corsi, D. M.; Murthy, N. N.; Young, V. G., Jr.; Karlin, K. D. Inorg. Chem. 1999, 38, 848–858.
- (22) Manor, B. C.; Ringenberg, M. R.; Rauchfuss, T. B. Inorg. Chem. 2014, 53, 7241-7247.
- (23) Tyeklár, Z.; Jacobson, R. R.; Wei, N.; Murthy, N. N.; Zubieta, J.; Karlin, K. D. J. Am. Chem. Soc. 1993, 115, 2677–2689.
- (24) Chen, C. H.; Liaw, W. F. Inorg. Synth. 2010, 35, 129-130.
- (25) Gloaguen, F.; Lawrence, J. D.; Schmidt, M.; Wilson, S. R.; Rauchfuss, T. B. J. Am. Chem. Soc. 2001, 123, 12518-12527.
- (26) Bignozzi, C. A.; Argazzi, R.; Schoonover, J. R.; Gordon, K. C.; Dyer, R. B.; Scandola, F. *Inorg. Chem.* **1992**, *31*, 5260–5267.
- (27) Kettle, S. F. A.; Diana, E.; Boccaleri, E.; Stanghellini, P. L. *Inorg. Chem.* **2007**, *46*, 2409–2416.
- (28) Denden, Z.; Ezzayani, K.; Saint-Aman, E.; Loiseau, F.; Najmudin, S.; Bonifácio, C.; Daran, J.-C.; Nasri, H. *Eur. J. Inorg. Chem.* **2015**, 2015, 2596–2610.
- (29) Closs, G. L.; Closs, L. E. J. Am. Chem. Soc. 1963, 85, 818-819.
- (30) Zhu, N.; Vahrenkamp, H. Chem. Ber. 1997, 130, 1241-1252.
- (31) Billing, D. E.; Dudley, R. J.; Hathaway, B. J.; Tomlinso, A. J. Chem. Soc. A 1971, 691–696.
- (32) Perraud, O.; Tommassino, J.-B.; Robert, V.; Khrouz, L.; Albela, B.; Bonneviot, L.; Dutasta, J.-P.; Martinez, A. *Dalton Trans.* **2013**, *42*, 1530–1535.
- (33) Schmitt, S.; Collin, C.; Bucher, V.; Maurel, J.-P.; Dutasta, A.; Martinez. Org. Biomol. Chem. 2015, 13, 2157–2161.
- (34) Becke, A. D. J. Chem. Phys. 1993, 98, 5648-5652.
- (35) Ding, S. Ph.D. Dissertation, Texas A&M University: College Station, TX, 2017.
- (36) Rao, G.; Tao, L.; Suess, D. L. M.; Britt, D. R. Nat. Chem. 2018, 10, 555-560.

## ■ NOTE ADDED AFTER ASAP PUBLICATION

Figure 8 was corrected on July 27, 2018.